THE JOURNAL OF PHYSICAL CHEMISTRY B

Article

pubs.acs.org/JPCB

Microrheological Investigations in Ionic Liquids Using Optical Trapping Techniques

Richard D. Dear, Emma K. Worrall, William D. Gault, and Grant A. D. Ritchie*

Department of Chemistry, Physical & Theoretical Chemistry Laboratory, University of Oxford, South Parks Road, Oxford OX1 3QZ, United Kingdom

ABSTRACT: In this paper, we demonstrate optical trapping of melamine particles ($d \approx 2.3$ μm) within the pure ionic liquid ethylammonium nitrate (EAN) and show the first microrheological investigations of these important compounds using this technique. By analyzing the power spectrum of a particle trapped in EAN, we monitor the variation in viscous drag that it experiences in proximity to the sample coverslip, showing excellent agreement with Faxén's law. We also demonstrate hydrodynamic coupling between pairs of trapped particles. Finally, we explore temperature-dependent viscosity changes in ~μL samples of EAN as a further example of microrheological investigations of ILs.

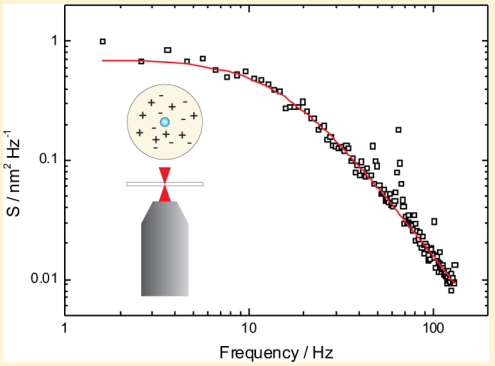

INTRODUCTION

In 1914, Walden reported the synthesis of ethylammonium nitrate (EAN),[1] credited as being the first deliberately developed room-temperature ionic liquid (IL). At first, these liquids were mainly of interest for electrochemical applications,[2] but since their proposal as organic solvents in the 1980s,[3,4] interest and research into these novel compounds has vastly increased. Often described as being "green" solvents,[5] their appeal comes from their extremely low volatilities,[6] large liquid range, high thermal and chemical stabilities,[7] and potential for decreasing the quantity of volatile organic compounds that are discharged into the atmosphere.[5] ILs show highly tunable properties through careful choice of the base cation and anion units and modification of any alkyl groups on the cation, allowing solubility, viscosity, density, and melting points to be altered.[8,9] This tunability has resulted in them being referred to as "designer solvents",[10] where properties can be tailored to specific applications. In addition to their use in organic synthesis, ILs have been used as industrial lubricants,[11] in chemical processing,[7] and in nanoparticle synthesis,[12] as well as showing an ability to absorb gases such as CO_2 with important applications in postcombustion capture.[13] For example, Ahosseini et al. report CO_2 mole fractions of up to 76% in [EMIM][Tf_2N] at ambient temperature under high-pressure conditions.[14]

Optical tweezers (OTs)[15] are a well-established technique for microrheological investigations of properties such as viscosity and flow.[16] A particular advantage of using OTs is the small sample volumes that are required (~10 μL) compared to conventional methods. This makes them ideal for the study of ILs, particularly when it is difficult to prepare large volumes of high-purity samples.[17] This technique also allows the investigation of local rather than bulk viscosities, which may be used to probe any sample microheterogeneity. Recently, the use of OTs as a tool for investigating IL solutions has been demonstrated in both aerosol and colloidal systems. Moore et al. have successfully trapped droplets of aqueous EAN solutions and spectroscopically characterized their change in composition in response to differing humidity conditions,[18] while Elmahdy et al. have trapped colloids in aqueous IL solutions ($\leq$0.01 M) to investigate how their pair interaction forces are affected by salt concentrations.[19]

In this article, we demonstrate for the first time that colloidal particles can be trapped within *pure* IL samples, and their behavior is used to investigate local properties, opening up a range of potential studies and applications. We first show trapping of melamine particles within EAN and characterize the system, verifying the expected overdamped behavior. We then demonstrate how these techniques allow viscosity changes within EAN samples to be measured, using Faxén's correction to the viscous drag of a particle close to a surface as an example. Using a dual-beam OTs setup, we then demonstrate hydrodynamic coupling between pairs of melamine particles before finally showing how single-beam OTs can be used to determine temperature-dependent viscosity changes in pure EAN samples.

Traditionally, the tracking of optically trapped particles has been performed using quadrant photodiodes (QPDs), which allow nanometer displacement measurements at rates of tens of kHz. Recently, however, the affordability of high-speed CMOS cameras, capable of frame rates of several kHz, has made them an attractive alternative for optical trapping applications.[20] Advantages over QPD tracking techniques include the ability to

Received: June 17, 2013
Revised: August 15, 2013
Published: September 4, 2013

   dx.doi.org/10.1021/jp405986q | *J. Phys. Chem. B* 2013, 117, 10567−10571

track multiple particles simultaneously and their relative ease of use compared to other tracking techniques. They are particularly suited to work in IL samples as the decrease in the typical resonance frequency of the trap, due to high IL viscosities, means that the higher temporal resolution offered by the QPD is unnecessary, and the high-speed camera frame rates are sufficient.

EXPERIMENTAL SECTION

Instrumental. The OT experiments were performed using the experimental setup shown in Figure 1. The output from a

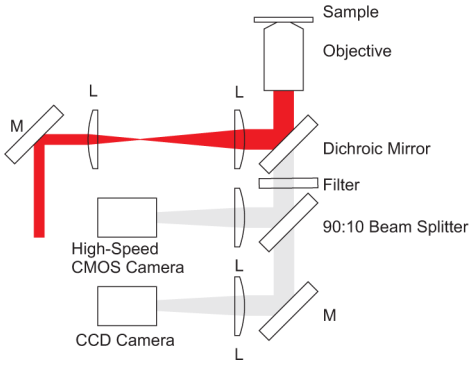

Figure 1. The experimental setup used for the work presented here, as described in the main text.

Laser Quantum Forte system (maximum power of 400 mW at 1064 nm, although with typically only ~20 mW used in the trap) was expanded by two lenses (L) in a 4f arrangement, before being focused into the sample using an oil immersion microscope objective (Nikon E Plan, 100 × /1.25). The sample was imaged using a CCD camera (Watec, WAT DM3S) with particle tracking performed using a high-speed CMOS camera (Dalsa Genie HM640). Illumination of the sample was achieved from above using a high-intensity fiber source (Thorlabs OSL1-EC). When dual-beam experiments were taking place, the beam was first split using polarization optics and then recombined following the protocol of Lee et al. (not shown in Figure 1).[21]

Sample Preparation. EAN, obtained from io-li-tec, was used for all of the results presented here without further purification. The 2.31 μm diameter melamine particles were purchased from microParticles GmbH with surface COOH functionalization. A typical sample consists of ~10 μL of EAN containing dispersed melamine particles, sandwiched between two glass coverslips separated by a custom vinyl spacer. We note that ILs may cause swelling of certain polymers, and therefore, care must be taken in order to select appropriate probe particles such that they are unaffected by the IL environment. Over the time scale of our measurements, the melamine particles used in this work were not swollen by being placed in EAN. When temperature-controlled experiments were taking place, an additional custom-made heater, consisting of a coil of resistance wire fixed to a coverslip using Araldite glue, was used on top of the standard sample. Temperature control was achieved by varying the voltage across the wire and monitored using a K-type thermocouple attached to the top of the slide. Calibration to determine the sample temperature from the thermocouple reading on the slide surface was performed separately.

Analysis. Data is typically acquired in 120 s periods in the form of particle coordinates, at 1600 frames per second using a custom LabVIEW program. Prior to calculating auto- and cross-correlation functions, the data were filtered to remove specific mechanical vibrational frequencies and then binned for averaging. Once the correlation functions were determined, an offset resulting from long-term experimental drift was subtracted. Power spectrum analysis was performed via a LabVIEW routine, which splits the data into 5 s intervals for analysis, as determined by Allan variance measurements,[22] and then fits it to eq 3, vide infra, using a least-squares fitting algorithm to return corner frequencies and trap stiffness values.

RESULTS AND DISCUSSION

Optical Trapping within EAN. The IL chosen for these experiments was EAN due to it being one of the most widely used and best-characterized ILs as well as being the first synthesized.[1] Its viscosity of 26.91 cP,[23] around 30× that of water, gives a corresponding increase in the OT time scale, as will now be demonstrated. In addition to this viscosity dependence, the change in refractive index when trapping in EAN rather than water will also influence the trap stiffness. The refractive index of 1.452 for EAN leads to a reduced refractive index contrast between the particle and the medium,[23] which is expected to decrease the trapping efficiency. This may also be reduced further by additional aberrations present when trapping in EAN due to the microscope objective being designed for use with water samples. By experimentally measuring and plotting trap stiffness as a function of power, a gradient of 0.66 ± 0.01 pN μm^{-1} mW^{-1} is determined for trapping in EAN, reduced from 0.92 ± 0.04 pN μm^{-1} mW^{-1} when water is the trapping medium, clearly indicating the reduced efficiency when trapping in the EAN sample. We will now show, however, that this does not prevent the stable trapping of colloidal particles in ILs, and we will show the use of this technique for microrheological investigation.

Position autocorrelation functions were determined by recording the position of a trapped 2.31 μm melamine particle in both EAN and water samples, and these are shown in Figure 2. The expected exponential decay for an overdamped system is observed, with the decay constant, τ, being given by

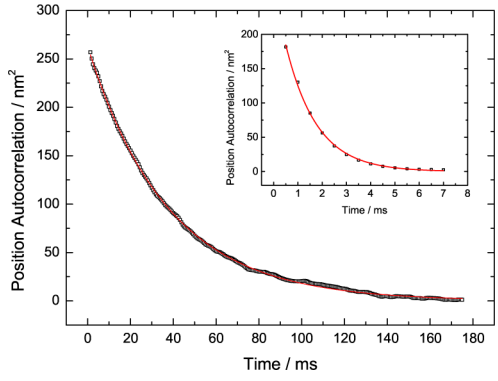

Figure 2. Position autocorrelation functions for a trapped 2.31 μm melamine particle in EAN (main) and water (inset), showing the expected exponential decay in each case. The differences in decay constant are due to the relative viscosities of the two media, as can be seen in eqs 1 and 2.

dx.doi.org/10.1021/jp405986q | J. Phys. Chem. B 2013, 117, 10567−10571

$$\tau = \frac{\gamma}{\kappa} \quad (1)$$

where γ is the friction coefficient of the particle and κ the stiffness of the trap.[24] For a spherical particle, the friction coefficient can be readily calculated via Stokes' law

$$\gamma = 6\pi\eta r \quad (2)$$

where η is the viscosity of the fluid and r the particle radius. Fitting to the example in Figure 2 yields a decay constant of $(3.74 \pm 0.01) \times 10^{-2}$ s^{-1}, corresponding to a trap stiffness of 15.66 ± 0.05 pN μm^{-1} for the EAN sample with a trapping power of 23.6 mW. One problem that becomes apparent due to the longer OTs time scale in EAN is the increased effect of mechanical noise. In addition, the longer time scales needed for data collection mean that the effects of long-term experimental drift become more important. These effects were minimized by using a vibrationally isolated table, reinforcing the cage assembly supporting the tweezers, and applying an electronic band-pass filter to the data. As a comparison to the IL trapping, an example autocorrelation function for a melamine particle trapped in water is also shown as an inset to Figure 2, for a trap stiffness of 15.14 ± 0.38 pN μm^{-1}. It is noted that in order to obtain this trap stiffness, less power was required than that for the IL case for the reasons already discussed. The smaller decay constant of $(1.28 \pm 0.03) \times 10^{-3}$ s^{-1} is consistent with the increase in viscosity of EAN compared to water once the slight difference in κ has been accounted for.

Having successfully shown the trapping of melamine particles in IL media, we will now demonstrate their use as microrheological probes. In order to determine physically useful properties from their Brownian dynamics, we will use the power spectrum method of trap stiffness determination.[25] The expected form of the power spectrum, $S(f)$, obtained by taking a Fourier transform of the position versus time data, is given by eq 3

$$S(f) = \frac{D/(2\pi^2)}{f_c^2 + f^2} \quad (3)$$

where D is the diffusion constant, equal to $k_B T/\gamma$, and f_c is the corner frequency, given by $f_c = \kappa/(2\pi\gamma)$. Fitting to this expression allows experimental corner frequencies to be determined, enabling accurate trap stiffnesses to be calculated. Figure 3 shows an example power spectrum for the EAN sample, with the expected low-frequency plateau and high-frequency tail tending to f^{-2}. A fit to eq 3, shown in red, returns a corner frequency of 15.1 Hz, indicating a trap stiffness of 55.7 ± 0.9 pN μm^{-1} for a laser power of 84.0 mW.

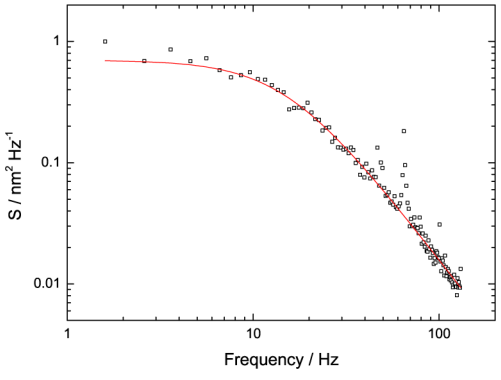

Figure 3. An example power spectrum for a 2.31 μm melamine particle in EAN. The power at the trap was 84mW, and a fit to eq 3 is shown in red.

Monitoring Faxén's Correction to Viscous Drag. Once the trap stiffness has been calculated for a given particle and sample, this technique can be used to monitor properties of the system, such as viscosity, as any changes will be reflected in a shift in the power spectrum corner frequency. One well-studied example of such a perturbation is a correction to the viscous drag on a sphere in close proximity to a plane surface. This effect can be determined for particle motion both perpendicular and parallel to the surface, as given by Faxén's law[26,27] and demonstrated by Leach et al.[28] This correction is highly dependent on the separation of the particle center and the surface, h. For particle motion parallel to a plane surface, this correction is given by

$$\gamma_{\text{Faxén}} \approx \frac{\gamma_0}{1 - \frac{9}{16}\left(\frac{r}{h}\right) + \frac{1}{8}\left(\frac{r}{h}\right)^3 - \frac{45}{256}\left(\frac{r}{h}\right)^4} \quad (4)$$

where $\gamma_{\text{Faxén}}$ is the corrected drag coefficient and γ_0 is the drag coefficient at large distances from the surface given by Stokes's law (eq 2). This correction, which is readily demonstrated for water samples, can be verified experimentally for the EAN samples by first trapping a particle at a large distance from any surface and then gradually decreasing the particle−coverslip separation. With knowledge of the optical trap stiffness, verified to be constant within the height range chosen by monitoring the variance in particle position at each point, the power spectrum method can be used to determine γ from the fitted corner frequency at each height. In each case, the actual particle height above the coverslip can be related to the change in stage height by considering the ratio of EAN and glass refractive indices.[29]

The ratios of these obtained friction coefficient values, γ, to the values given by Stokes' Law, γ_0, for a melamine particle trapped in EAN at a series of trapping heights are given in Figure 4. The expected increase in viscous drag coefficient at reduced particle−coverslip separations is seen, with γ tending to γ_0 at larger separations. When analyzing the data, we follow Vermeulen et al. and define $h = h_m + \Delta h$, where h_m is the measured height and Δh allows for the fact that the absolute particle−coverslip separation at the closest measurement point is unknown.[27] Fitting to this modified expression returns a Δh

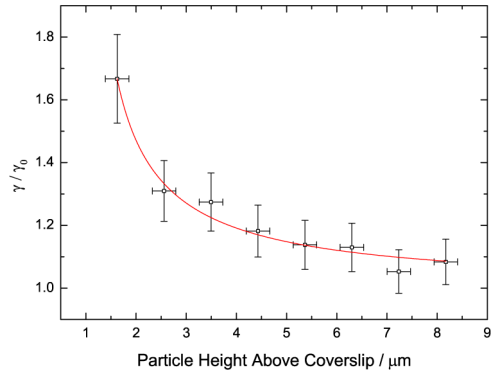

Figure 4. Variation of the friction coefficient for a trapped melamine particle in EAN relative to its bulk value as a function of particle height above the sample coverslip. A best fit to the expected form, given by Faxén's law, is shown in red.

dx.doi.org/10.1021/jp405986q | J. Phys. Chem. B 2013, 117, 10567−10571

value of 1.6 μm as the minimum particle−coverslip separation, slightly larger than r, as expected. This offset was used to determine the absolute height values shown in Figure 4.

Hydrodynamic Coupling. The increased OT time scale in EAN compared to that of water is also apparent in the hydrodynamic coupling between trapped particles, observed and quantified by utilizing a dual-beam OTs setup. The dual-beam tweezers allow two particles to be simultaneously trapped at varying separations, and by examining the position cross-correlation function between them, their hydrodynamic coupling can be studied. The resulting cross-correlation functions exhibit a time-delayed anticorrelation, as demonstrated by Meiners and Quake,[24] which varies in magnitude with interparticle spacing and can be understood using Langevin dynamics. This time delay is observed despite the assumed instantaneous propagation of forces through the fluid and instead results from the relaxation time of the optical trap. Calculation of this function along the longitudinal axis between two trapped particles gives the following cross-correlation expression

$$\langle R_1(t)R_2(0)\rangle = \frac{k_B T}{2\kappa}(e^{-(1+\epsilon)t/\tau} - e^{-(1-\epsilon)t/\tau}) \quad (5)$$

where R_1 and R_2 describe the positions of particles 1 and 2 along the interparticle axis, $\epsilon = 3r/2E$, and E is the mean separation between the two particles.[24] It can be shown that the minimum in the cross-correlation function occurs at $t \approx \tau$ and therefore appears on the order of a millisecond in water samples but at much longer time scales in EAN. Analysis assumes a no-slip boundary condition between the particle and the IL, though it would be interesting to investigate potential violations of no-slip boundary conditions in other IL media.[30] The longitudinal position cross-correlation is shown in Figure 5

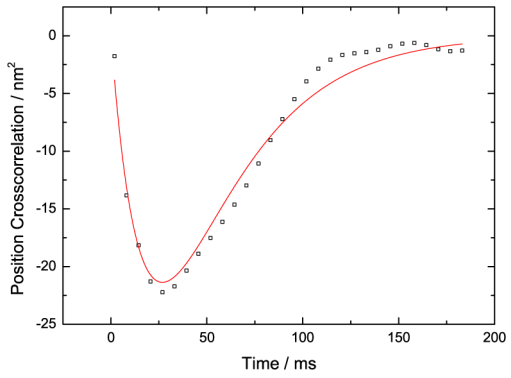

Figure 5. A measured position cross-correlation function for two melamine particles trapped 5.53 μm apart using a dual-beam setup. The expected form of the cross-correlation function, determined following the approach of Meiners and Quake,[24] is shown in red.

for two melamine particles trapped in EAN at a separation of 5.53 ± 0.02 μm. By calibrating our data from the single-particle autocorrelation functions, the expected form of the cross-correlation can be determined exactly from eq 5 and is shown to demonstrate excellent agreement with no variable fitting parameters.

Quantifying Temperature-Dependent Viscosity Changes in EAN. Having verified that OTs methods can be used to monitor effects such as viscous drag corrections in IL samples and that multiple particle effects such as hydrodynamic coupling can be measured and understood, we now show that these techniques can be extended to consider the effect of temperature on EAN systems. The temperature dependence of the dynamic viscosity of EAN has been previously measured using macrorheological techniques, with Poole et al. observing viscosity reductions of up to 50% just a few tens of degrees above room temperature[23] and reporting the following relationship

$$\ln \eta = A_1 + A_2 T \quad (6)$$

where T is the temperature in degrees Celsius and A_1 and A_2, determined from a fit to their experimental data, are constants equal to 4.33 and -3.49×10^{-2}, respectively.

In order to investigate this trend using OTs, a custom-built heater, consisting of a coil of resistance wire fixed to a coverslip using Araldite glue, is attached to the top of a sample slide. The sample temperature is measured using a K-type thermocouple situated on the slide surface with conversion between the slide surface and sample temperatures achieved by prior calibration. By utilizing the techniques already described and knowledge of the room-temperature viscosity and trap stiffness, we confirm the same trend as Poole et al. by recording power spectra and determining EAN viscosities at a range of sample temperatures, as shown in Figure 6. Fitting to our experimental data yields a

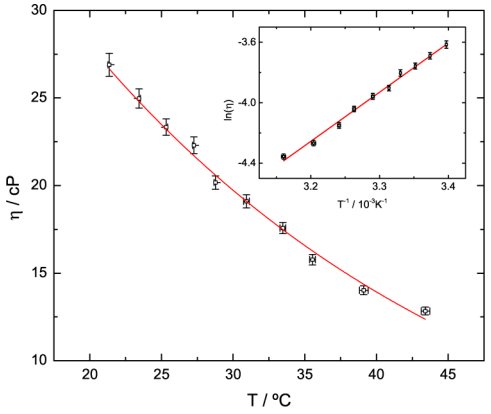

Figure 6. EAN viscosity measurements as a function of sample temperature, determined by monitoring changes in the power spectrum of a trapped melamine particle. (Inset) A plot of ln (η) against T^{-1} allows the activation energy for viscous flow to be determined.

value of A_2 of $-(3.48 \pm 0.12) \times 10^{-2}$, in excellent agreement with the values obtained by macrorheological techniques. An Arrhenius-like law can also be used to interpret the temperature-dependent viscosity changes in ILs,[31] allowing the activation energy for viscous flow, E_a, to be determined via a plot of ln (η) against T^{-1}, as shown in the inset of Figure 6. A linear fit returns an activation energy of 27.0 ± 0.8 kJ·mol^{-1}, in good agreement with the previously reported value of 24.26 ± 1.91 kJ·mol^{-1}.[32]

CONCLUSIONS

This clear demonstration of the applicability of OT in microrheological investigations of ILs shows great promise for further study. Advantages over existing techniques include the need for only small sample volumes, which is of importance due to the difficulties in preparing large quantities of pure ILs. In addition, they offer the potential to investigate any sample microheterogeneity that is not possible with existing bulk

dx.doi.org/10.1021/jp405986q | J. Phys. Chem. B 2013, 117, 10567−10571

techniques. The simplicity of the high-speed camera setup allows investigations using a wide range of cell designs as long as they are sufficiently well illuminated for high frame rate capture. As well as including temperature-controlled slides, as demonstrated here, experiments investigating CO_2 capture and its effect on IL viscosity could easily be performed with a suitable cell design, potentially also incorporating real-time optical spectroscopy. The technique also lends itself to further examination of the effect of impurities such as water on the physical properties of IL samples.[33]

AUTHOR INFORMATION

Corresponding Author

*E-mail: grant.ritchie@chem.ox.ac.uk.

Notes

The authors declare no competing financial interest.

ACKNOWLEDGMENTS

The authors would like to thank Dr. Arran Curran for allowing us to use his LabVIEW particle tracking routines.

REFERENCES

(1) Walden, P. Ueber die Molekulargrösse und Elektrische Leitfähigkeit Einiger Geschmolzenen Salze. *Bull. Acad. Imp. Sci. St.-Petersbourg* **1914**, *8*, 405−422.

(2) Hurley, F. H.; Wier, T. P. The Electrodeposition of Aluminum from Nonaqueous Solutions at Room Temperature. *J. Electrochem. Soc.* **1951**, *98*, 207−212.

(3) Fry, S. E.; Pienta, N. J. Effects of Molten Salts on Reactions. Nucleophilic Aromatic Substitution by Halide Ions in Molten Dodecyltributylphosphonium Salts. *J. Am. Chem. Soc.* **1985**, *107*, 6399−6400.

(4) Boon, J. A.; Levisky, J. A.; Pflug, J. L.; Wilkes, J. S. Friedel−Crafts Reactions in Ambient-Temperature Molten Salts. *J. Org. Chem.* **1986**, *51*, 480−483.

(5) Zhao, H.; Xia, S.; Ma, P. Use of Ionic Liquids as 'Green' Solvents for Extractions. *J. Appl. Chem. Biotechnol.* **2005**, *80*, 1089−1096.

(6) Earle, M. J.; Seddon, K. R. Ionic Liquids. Green Solvents for the Future. *Pure Appl. Chem.* **2000**, *72*, 1391−1398.

(7) Brennecke, J. F.; Maginn, E. J. Ionic Liquids: Innovative Fluids for Chemical Processing. *AIChE J.* **2001**, *47*, 2384−2389.

(8) Plechkova, N. V.; Seddon, K. R. In *Methods and Reagents for Green Chemistry: An Introduction*; Tundo, P., Perosa, A., Zecchini, F., Eds.; John Wiley & Sons, Inc.: Hoboken, NJ, 2007.

(9) Holbrey, J. D.; Seddon, K. R. The Phase Behaviour of 1-Alkyl-3-methylimidazolium Tetrafluoroborates; Ionic Liquids and Ionic Liquid Crystals. *J. Chem. Soc., Dalton Trans.* **1999**, 2133−2140.

(10) Freemantle, M. Designer Solvents — Ionic Liquids May Boost Clean Technology Development. *Chem. Eng. News* **1998**, *76*, 32−37.

(11) Bermúdez, M.-D.; Jiménez, A.-E.; Sanes, J.; Carrión, F.-J. Ionic Liquids as Advanced Lubricant Fluids. *Molecules* **2009**, *14*, 2888−2908.

(12) Estruga, M.; Domingo, C.; Domènech, X.; Ayllón, J. A. Zirconium-Doped and Silicon-Doped TiO_2 Photocatalysts Synthesis from Ionic-Liquid-Like Precursors. *J. Colloid Interface Sci.* **2010**, *344*, 327−333.

(13) Brennecke, J. F.; Gurkan, B. E. Ionic Liquids for CO_2 Capture and Emission Reduction. *J. Phys. Chem. Lett.* **2010**, *1*, 3459−3464.

(14) Ahosseini, A.; Ortega, E.; Sensenich, B.; Scurto, A. M. Viscosity of n-Alkyl-3-methyl-imidazolium Bis(trifluoromethylsulfonyl)amide Ionic Liquids Saturated with Compressed CO_2. *Fluid Phase Equilib.* **2009**, *286*, 72−78.

(15) Ashkin, A.; Dziedzic, J. M.; Bjorkholm, J. E.; Chu, S. Observation of a Single-Beam Gradient Force Optical Trap for Dielectric Particles. *Opt. Lett.* **1986**, *11*, 288−290.

(16) Yao, A.; Tassieri, M.; Padgett, M.; Cooper, J. Microrheology with Optical Tweezers. *Lab Chip* **2009**, *9*, 2568−2575.

(17) Scammells, P. J.; Scott, J. L.; Singer, R. D. Ionic Liquids: The Neglected Issues. *Aust. J. Chem.* **2005**, *58*, 155−169.

(18) Moore, L. J.; Summers, M. D.; Ritchie, G. A. D. Optical Trapping and Spectroscopic Characterisation of Ionic Liquid Solutions. *Phys. Chem. Chem. Phys.* **2013**, *15*, 13489−13498.

(19) Elmahdy, M. M.; Gutsche, C.; Kremer, F. Forces within Single Pairs of Charged Colloids in Aqueous Solutions of Ionic Liquids as Studied by Optical Tweezers. *J. Phys. Chem. C* **2010**, *114*, 19452−19458.

(20) Keen, S.; Leach, J.; Gibson, G.; Padgett, M. J. Comparison of a High-Speed Camera and a Quadrant Detector for Measuring Displacements in Optical Tweezers. *J. Opt. A: Pure Appl. Opt.* **2007**, *9*, S264−S266.

(21) Lee, W. M.; Reece, P. J.; Marchington, R. F.; Metzger, N. K.; Dholakia, K. Construction and Calibration of an Optical Trap on a Fluorescence Optical Microscope. *Nat. Protoc.* **2007**, *2*, 3226−3238.

(22) Gibson, G. M.; Leach, J.; Keen, S.; Wright, A. J.; Padgett, M. J. Measuring the Accuracy of Particle Position and Force in Optical Tweezers Using High-Speed Video Microscopy. *Opt. Express* **2008**, *16*, 14561−14570.

(23) Poole, C. F.; Kersten, B. R.; Ho, S. S.; Coddens, M. E.; Furton, K. G. Organic Salts, Liquid at Room Temperature, as Mobile Phases in Liquid Chromatography. *J. Chromatogr., A* **1986**, *352*, 407−425.

(24) Meiners, J.-C.; Quake, S. R. Direct Measurement of Hydrodynamic Cross Correlations between Two Particles in an External Potential. *Phys. Rev. Lett.* **1999**, *82*, 2211−2214.

(25) Berg-Sørensen, K.; Flyvbjerg, H. Power Spectrum Analysis for Optical Tweezers. *Rev. Sci. Instrum.* **2004**, *75*, 594−612.

(26) Faxén, H. Die Bewegung einer Starren Kugel Längs der Achse eines mit Zäher Flüssigkeit Gefüllten Rohres. *Ark. Mat., Astron. Fys.* **1923**, *17*, 1−28.

(27) Vermeulen, K. C.; Wuite, G. J. L.; Stienen, G. J. M.; Schmidt, C. F. Optical Trap Stiffness in the Presence and Absence of Spherical Aberrations. *Appl. Opt.* **2006**, *45*, 1812−1819.

(28) Leach, J.; Mushfique, H.; Keen, S.; Di Leonardo, R.; Ruocco, G.; Cooper, J.; Padgett, M. Comparison of Faxén's Correction for a Microsphere Translating or Rotating Near a Surface. *Phys. Rev. E* **2009**, *79*, 026301−1−4.

(29) Fällman, E.; Axner, O. Influence of a Glass−Water Interface on the On-Axis Trapping of Micrometer-Sized Spherical Objects by Optical Tweezers. *Appl. Opt.* **2003**, *42*, 3915−3926.

(30) Fu, H.; Shenoy, V.; Powers, T. Role of Slip Between a Probe Particle and a Gel in Microrheology. *Phys. Rev. E* **2008**, *78*, 061503/1−061503/14.

(31) Jacquemin, J.; Husson, P.; Padua, A. A. H.; Majer, V. Density and Viscosity of Several Pure and Water-saturated Ionic Liquids. *Green Chem.* **2006**, *8*, 172−180.

(32) Capelo, S. B.; Méndez-Morales, T.; Carrete, J.; López Lago, E.; Vila, J.; Cabeza, O.; Rodrguez, J. R.; Turmine, M.; Varela, L. M. Effect of Temperature and Cationic Chain Length on the Physical Properties of Ammonium Nitrate-Based Protic Ionic Liquids. *J. Phys. Chem. B* **2012**, *116*, 11302−11312.

(33) Seddon, K. R.; Stark, A.; Torres, M.-J. Influence of Chloride, Water, and Organic Solvents on the Physical Properties of Ionic Liquids. *Pure Appl. Chem.* **2000**, *72*, 2275−2287.